RESEARCH MEMORANDUM

TRANSONIC FLUTTER CHARACTERISTICS OF AN ASPECT-RATIO-4,

45° SWEPTBACK, TAPER-RATIO-0.2 PLAN FORM

By John R. Unangst

Langley Research Center
Langley Field, Va.

NATIONAL ADVISORY COMMITTEE
FOR AERONAUTICS

WASHINGTON December 1959
Declassified January 12, 1961

NATIONAL AERONAUTICS AND SPACE ADMINISTRATION

TECHNICAL MEMORANDUM X-136

TRANSONIC FLUTTER CHARACTERISTICS OF AN ASPECT-RATIO-4,

45° SWEPTBACK, TAPER-RATIO-0.2 PLAN FORM*

By John R. Unangst

SUMMARY

The results of several flutter investigations to determine the
effects of plan-form variations on the flutter characteristics of thin
cantilevered wings at transonic Mach numbers have been reported pre-
viously. In the present investigation the data are extended to include
a wing having an aspect ratio of 4, 45° of sweepback, and a taper ratio
of 0.2. The data were obtained in the Langley transonic blowdown tunnel
over a Mach number range from 0.6 to 1.4.

The experimental results indicate an abrupt and rather large increase
in both a flutter-speed parameter and a flutter-frequency parameter as
the Mach number is increased from 1.05 to 1.10. The foregoing is inter-
preted as indicating a marked change in the flutter mode. Calculated
flutter speeds, based on incompressible-flow aerodynamic coefficients,
were too high by 20 percent or more throughout the subsonic Mach number
range of the investigation. Calculated flutter frequencies were about
7 percent too high at a Mach number of 0.65 and were about 20 percent
too high at a Mach number of 0.9. No significant independent effects
of thickness were indicated for the plan form investigated as the thick-
ness was changed from 3 to 4 percent chord.

INTRODUCTION

Several flutter investigations have been conducted in the Langley
transonic blowdown tunnel in order to determine the effects of plan-
form variations on the flutter characteristics of thin cantilevered wings
at transonic Mach numbers. The results of two of these investigations
are reported in references 1 and 2. In reference 1, wings having various
aspect ratios and sweepback angles with a constant taper ratio of 0.6
were investigated. Reference 2 extended the data of reference 1 for the

---

aspect-ratio-4, 45° sweptback plan form tc include a taper ratio of 1.0. The present investigation represents a further extension of the data of reference 1 for the aspect-ratio-4, 45° sweptback wing to include a taper ratio of 0.2.

Data for the present investigation were obtained in the Langley transonic blowdown tunnel at Mach numbers from 0.6 to 1.4 with full-span sting-mounted models. In order to obtain flutter throughout the Mach number range, it was necessary to use two series of models which had different levels of stiffnesses.

SYMBOLS

a   distance perpendicular to quarter-chord line, in wing semi-chords, from midchord to elastic-axis position; positive for elastic axis behind midchord

A   aspect ratio including body intercept, $\dfrac{(\text{Span})^2}{\text{Area}}$

A_p panel aspect ratio, $\dfrac{(\text{Exposed semispan})^2}{\text{Exposed panel area}}$

b   local semichord perpendicular tc quarter-chord line, ft

b_r semichord perpendicular to quarter-chord line at intersection of quarter-chord line and wing root, ft

b_s semichord measured streamwise at intersection of wing root and fuselage, ft

b_t streamwise semichord at wing tip, ft

c   local streamwise chord, ft

f   frequency of vibration, cps

$f_{h,i}$ measured coupled bending frequencies (i = 1, 2, 3), cps

f_t measured first coupled torsional frequency, cps

f_α uncoupled first torsional frequency,

$$f_t \left[1 - \frac{\left(\dfrac{x_\alpha}{r_\alpha}\right)^2}{1 - \left(\dfrac{f_{h,1}}{f_t}\right)^2} \right]^{1/2}$$

where $\left(\dfrac{x_\alpha}{r_\alpha}\right)^2$ is evaluated at $\eta = 0.75$ station, cps

EI bending stiffness, lb-in.^{2}

GJ torsional stiffness, lb-in.^{2}

g_h structural damping coefficient associated with the first coupled bending mode

I_α mass moment of inertia per unit length of wing along quarter-chord line, measured about elastic axis, slug-ft^2/ft

k_r reduced frequency based on semichord of effective wing root, $b_r \omega / V_n$

l length of wing panel outside fuselage, measured along quarter-chord line, ft

l' length of wing panel outside fuselage measured perpendicular to streamwise root chord, ft

M Mach number

m mass of wing per unit length along quarter-chord line, slugs/ft

$\bar{m}$ total mass of exposed wing panel, slugs

q dynamic pressure, lb/sq in.

r_α nondimensional radius of gyration about elastic axis measured perpendicular to quarter-chord line, $\left(I_\alpha / mb^2\right)^{1/2}$

T time, sec

V stream velocity, ft/sec

V_n component of stream velocity normal to quarter-chord line, ft/sec

V_e/V_R flutter-speed ratio

v volume of air within a conical frustum having streamwise wing root chord as the lower base diameter and streamwise wing tip chord as the upper base diameter, $\frac{1}{3}l'\pi\left(b_s^2 + b_s b_t + b_t^2\right)$, cu ft

x_α distance in wing semichords from elastic axis to center of gravity, measured perpendicular to quarter-chord line, positive for center of gravity behind elastic axis

η nondimensional coordinate along quarter-chord line, measured from intersection of quarter-chord line and fuselage, fraction of quarter-chord-line length

μ mass ratio evaluated at $\eta = 0.75$ station, $m/\pi\rho b^2$

$\bar{\mu}$ mass ratio evaluated for entire wing panel, $\bar{m}/\rho v$

λ taper ratio, $\dfrac{\text{Streamwise tip chord}}{\text{Chord in plane of symmetry}}$

λ_p exposed panel taper ratio, $\dfrac{\text{Streamwise tip chord}}{\text{Root chord of exposed wing}}$

Λ sweepback angle of quarter-chord line, deg

ρ air density, slugs/cu ft

ω angular frequency of vibration, $2\pi f$, radian/sec

$\omega_{h,i}$ angular bending frequencies (i = 1, 2, 3), $2\pi f_{h,i}$, radian/sec

ω_α angular uncoupled torsional frequency, $2\pi f_\alpha$, radian/sec

Subscripts:

e   experimental values

R   calculated reference values

MODELS

Model Geometry and Construction

The models employed in the investigation had an aspect ratio of 4, 45° of sweepback of the quarter-chord line, and a taper ratio of 0.2. Drawings of the plan form are presented in figure 1. In all, six models were used. Models 1 and 2 had approximately 4-percent-thick streamwise airfoil sections, and models 1A, 2A, 3A, and 4A had approximately 3-percent-thick streamwise airfoil sections. Model 4A was not tested but was employed solely for obtaining the mass properties of the thinner models. The purpose in using wings of two different thicknesses was to provide two sets of stiffnesses so that flutter could be obtained over a larger Mach number range. It was anticipated that the independent effects of thickness on the flutter characteristics would be negligible.

Each model was machined from a solid block of Consoweld, a resin-impregnated paper (ref. 3). The 0.38-inch-thick fuselage block in the center of each model (fig. 1(a)) was made flat and rectangular in shape to facilitate clamping in the sting support used in the wind-tunnel tests.

Physical Properties

A tabulation of some of the physical properties of the models is given in table I. Spanwise variations of model-section properties are tabulated for a single representative panel (exposed semispan) of each thickness ratio. Thus, in table I(a) the section properties of the right panel of model 4A are considered to be representative of all the 3-percent-thick models and, similarly, the properties of the left panel of model 1 (table I(b)) are considered to be representative of the two 4-percent-thick models. The measured natural-vibration frequencies and the node lines are shown in table I and figure 1(b), respectively, for all models used in the wind-tunnel tests.

For determination of the elastic-axis location a, the model was clamped along a line perpendicular to the quarter-chord line and passing through the intersection of the wing trailing edge and the root. The chordwise position at which a concentrated bending load produced no twist in the wing was determined at several spanwise stations, and a straight line faired through these points was taken as the elastic-axis location. The parameters which define the mass per unit length, center-of-gravity location, and radius of gyration (m, x_α, r_α, respectively) were determined from measurements made on strips cut perpendicular to the quarter-chord line.

The total wing-panel mass $\bar{m}$ was determined by weighing the entire panel before cutting it into strips. Structural damping coefficients were determined from the decrement of free-bending vibrations in still air. An average value of these coefficients is presented in table I for each thickness-ratio series of models. The natural-vibration frequencies listed in table I and the associated node lines (fig. 1(b)) were obtained from forced vibration tests. For these tests each model was clamped to a steel bench so that each wing panel could be considered as being cantilevered from the fuselage block. An electromagnetic shaker, located near the wing root, was used to excite the panels, and salt crystals sprinkled on the panel were used to identify the node lines. Values of the uncoupled torsional frequencies f_α shown in table I were inferred from the measured torsional frequencies by means of the simple formula taken from reference 4 and given in the "Symbols" section herein.

The spanwise variation of bending and torsional stiffnesses for one wing panel of a 4-percent-thick model is plotted in figure 2. These data were obtained from load-deflection measurements made along the elastic axis.

APPARATUS AND TESTS

Wind Tunnel

The flutter tests were conducted in the Langley transonic blowdown tunnel. This tunnel is equipped with a slotted, octagonal test section which measures approximately 26 inches between flats. During operation of the tunnel, a preselected Mach number is set by means of a variable orifice downstream of the test section. This Mach number is maintained approximately constant (after the orifice is choked) while the stagnation pressure, and thus the density, is increased. The maximum stagnation pressure is 75 lb/sq in. The static-density range is approximately 0.001 to 0.012 slug/cu ft; Mach numbers from subsonic values to a maximum of about 1.4 may be obtained. It should be noted that, because the stagnation temperature continually decreases during a run as a result of expansion of the air in the reservoir, the test-section velocity is not defined uniquely by the Mach number. (A run is defined as one operation of the tunnel from valve opening to valve closing.) The orifice area may be varied to some extent during a run, thus providing some additional flexibility in operating characteristics. The operating characteristics of the tunnel in terms of dynamic pressure and Mach number are indicated in figure 3 for four different orifice settings. The additional information shown in figure 3 will be discussed in subsequent sections of this paper.

Support System

The models were supported in the tunnel by a 3-inch-diameter sting fuselage. The nose of the sting extended into the tunnel entrance cone, where the flow is always subsonic, to prevent the formation of a bow shock wave which might reflect from the tunnel walls onto the model. The complete support system weighed about 290 pounds and was considered to form a rigid mount for the models since the mass of the system was very large compared with the mass of a model. The fundamental frequency of the support system was approximately 15 cycles/sec.

Instrumentation

Electrical strain gages were mounted on the surface of each wing panel near the root. These gages were oriented so as to indicate as nearly as possible the separate bending and torsional deflections of the wings. A multichannel recording oscillograph was employed to record the time history of the strain-gage signals, tunnel stagnation pressure and temperature, and test-section static pressure during the runs. A pair of cathode-ray oscilloscopes were employed in connection with the strain gages to aid the observer in detecting the occurrence of flutter during the tests. The strain-gage signals were fed to the oscilloscopes in such a way that a Lissajous figure appeared at flutter.

Tests

The objectives of the wind-tunnel tests were to determine the frequency and the airspeed and density at flutter over a range of transonic Mach numbers. Flutter is obtained in the blowdown tunnel by gradually increasing the stagnation pressure until flutter is definitely identified by the observer, either by visual observation of the model or with the aid of the aforementioned oscilloscopes. Once flutter is obtained, the stagnation pressure is held constant momentarily and then is quickly reduced. During the present investigation it was found that the flutter boundary of the models was so located within the operating range of the tunnel that flutter at Mach numbers above about 1.05 could not be obtained without flutter first being encountered at subsonic speeds (about $M_e = 0.70$ to 0.95). This situation is illustrated in figure 3 in which the flutter boundary for the 3-percent-thick wings is superimposed on the curves of tunnel-operating characteristics. The tunnel-operating curves for two different orifice settings are shown in figure 3 to intersect the flutter boundary at three points, first near $M = 0.7$ where flutter would start, next near $M = 1.07$ where flutter would stop, and finally at some higher supersonic Mach number where flutter would start again. In order to obtain flutter at supersonic Mach numbers, the stagnation pressure was increased rapidly through the subsonic part of the flutter

region, thus giving a start and stop of flutter, and then increased gradually until supersonic flutter was obtained.

METHOD OF ANALYSIS

The method used to calculate flutter speeds for the present paper is based on the method presented in reference 4. In brief, this method employs two-dimensional, incompressible aerodynamic coefficients in a Rayleigh type of analysis. The aerodynamic coefficients are based on the component of the free-stream velocity normal to the quarter-chord line. In the present calculation the flutter mode was approximated by the superposition of the first three uncoupled mode shapes of the wing (two bending and one torsional). The mode shapes were calculated from the measured stiffness data (fig. 2) and the measured mass and inertia data (table I) by the method of reference 5. Since measured stiffness data were not available for the 3-percent-thick wings, the nondimensional mode shapes calculated for the 4-percent-thick wings are assumed to be applicable to all models employed in the investigation. Although it was believed that the mode shapes calculated for the single 4-percent-thick wing would adequately represent all of the wings tested, it was felt that the corresponding calculated frequencies probably would not be adequate. Consequently, measured values of the natural frequencies are applied in the present flutter-speed calculations. The measured (coupled) torsional frequencies were adjusted to the uncoupled values by means of the simple formula given in reference 4 and in the symbols; the measured frequencies of the predominantly bending modes were taken to be the uncoupled values.

The effective root and tip chords of the exposed wing are defined in the present analysis as the chords perpendicular to the quarter-chord line at the intersection of the quarter-chord line with the actual root and tip, respectively. The effective wing length is defined as the perpendicular distance between the effective root and tip chords. The solutions of the flutter determinant were carried out by automatic punch-card computing equipment in such a way that a plot of structural damping coefficient g_h against flutter-speed coefficient $V_R/b_r\omega_\alpha$ could be made. A more detailed discussion of the method of solving the flutter determinant is given in reference 6.

RESULTS AND DISCUSSION

Presentation of Data

The analytical and experimental results of the investigation are presented in table II and are plotted in figures 4 to 8. In table II

the first column gives the identification numbers of the models employed in obtaining the data. The second column shows the run number and the third column shows the chronology of the data points obtained during a particular run. The fourth and fifth columns contain a code system which describes each data point. This code system is defined at the bottom of table II(a). The column labeled f_α gives the uncoupled torsion frequency for the wing panel associated with the data point. For data points which involve the simultaneous start or stop of flutter for both panels of a given model, the average f_α for the model is presented.

In figures 4 to 8, data indicating the start of flutter are shown by open symbols; data indicating the end of flutter as the dynamic pressure was increasing are shown by flagged symbols. Data showing a no-flutter condition at the maximum dynamic pressure attained during a run are shown by shaded symbols. In some of the runs a period of intermittent sinusoidal oscillations was obtained preceding flutter which obscured the exact start of flutter. This behavior is referred to as low damping (ref. 1) and the regions of low damping are indicated in the data by dashed lines preceding the flutter point.

Experimental Results

The variation with Mach number of the dynamic pressure required for flutter for the 3- and 4-percent-thick wings is presented in figure 4. At Mach numbers below 0.75, data were obtained with the 3-percent-thick wings. At the higher subsonic Mach numbers, the flutter boundary for the 3-percent-thick wings was at lower dynamic pressures than that at which the tunnel would operate and the 4-percent-thick wings were fluttered in this region. At Mach numbers above 1.1 the 4-percent-thick wings were too stiff to flutter within the dynamic-pressure range available and the 3-percent-thick wings were used to obtain flutter points in this region.

The data from figure 4 are presented in figure 5 in the form of the parameter $\dfrac{V_e}{b_s \omega_\alpha \sqrt{\mu_e}}$ as a function of Mach number. It should be noted that for a given plan form

$$\frac{V_e}{b_s \omega_\alpha \sqrt{\mu_e}} \propto \sqrt{\frac{q_e \, l}{\overline{m} \omega_\alpha{}^2}}$$

Thus, the parameter adjusts the dynamic pressure at flutter by the mass and torsional frequency characteristics of the models. The correlation of the data for the 3- and 4-percent-thick wings by use of this parameter (fig. 5) suggests that there are no significant independent effects

of thickness ratio on the flutter characteristics of the plan form investigated for the values of thickness ratio employed.

The flutter boundary in figure 5 is characterized by a dip in the high subsonic Mach number region, with a minimum at about M_e = 0.9, followed by a gradual increase in $\dfrac{V_e}{b_s \omega_\alpha \sqrt{\bar{\mu}_e}}$ with Mach number from this point up to about M_e = 1.05. Between M_e = 1.05 and M_e = 1.1, a very rapid increase in $\dfrac{V_e}{b_s \omega_\alpha \sqrt{\bar{\mu}_e}}$ occurs, after which $\dfrac{V_e}{b_s \omega_\alpha \sqrt{\bar{\mu}_e}}$ increases gradually with Mach number from M_e = 1.1 to M_e = 1.4.

The flutter frequencies, normalized by the appropriate uncoupled torsional frequencies, are shown plotted against Mach number in figure 6. The agreement of the data for the 3- and 4-percent-thick wings suggests that the flutter modes for models of both thickness ratios were essentially the same, at least up to M_e = 1.08. Comparison at higher Mach numbers could not be obtained because the 4-percent-thick wings could not be fluttered above M_e = 1.08.

A very rapid increase in flutter frequency between Mach numbers of 1.05 and 1.10 is indicated in figure 6. The trend of the flutter frequencies between Mach numbers of 1.05 and 1.10 corresponds to the trends of dynamic pressure and $\dfrac{V_e}{b_s \omega_\alpha \sqrt{\bar{\mu}_e}}$ at flutter in the same Mach number range (figs. 4 and 5, respectively). Thus, a rather marked change in the flutter mode in this Mach number range is suggested. It should be noted that data points were obtained throughout the region of transition from one flutter mode to the other.

An interesting illustration of the occurrence of the previously discussed change in the flutter mode may be seen by referring to the data for run 10 in table II(a) and following the tunnel operating path for this run in figure 3. Sections from the oscillograph record for run 10 are presented in figure 9. From figures 3 and 9 it can be seen that, after the initial start of flutter at point 10-1 (fig. 9(a)), the wing flutters continuously in the lower frequency mode until point 10-2a, 2b was reached (fig. 9(b)). At this point the flutter frequency abruptly increased to a considerably higher value and flutter continued in this higher frequency mode as the dynamic pressure and Mach number were increased to the maximum values for the run, corresponding to point 10-4 (fig. 9(c)). At this point the Mach number was gradually reduced, so that the lower frequency flutter mode was reestablished at point 10-5a, 5b (fig. 9(d)).

Comparison With Calculated Results

The ratio of experimental flutter speed to calculated flutter speed V_e/V_R plotted against Mach number is presented in figure 7 for the plan form investigated herein. It is apparent from figure 7 that the calculated flutter speeds are higher by 20 percent or more than the experimental flutter speeds throughout the subsonic Mach number range of the investigation. Since incompressible aerodynamic coefficients were used in the flutter-speed calculation, it was expected that the agreement between experimental and calculated flutter speeds would not be good at supersonic Mach numbers, an expectation which is borne out by the results shown in figure 7. The reasons for the overestimation of the flutter speeds at subsonic Mach numbers are not, however, apparent. The proximity of the third bending frequencies to the first torsion frequencies (table I) suggested the inclusion of the third bending degree of freedom in the analysis in an effort to lower the calculated flutter speeds. However, very little change in calculated flutter speeds resulted from the use of the third bending mode in the analysis. Hence, the calculated flutter characteristics presented involve only the first three uncoupled wing modes.

The ratio of experimental flutter frequency to calculated flutter frequency ω_e/ω_R is shown in figure 8 plotted against Mach number. The calculated flutter frequencies were higher than the experimental values by about 7 percent at a Mach number of 0.65 and by about 20 percent at a Mach number of 0.9.

Effects of Taper Ratio

A comparison of results obtained with the present taper-ratio-0.2 plan form with those for similar plan forms having taper ratios of 0.6 and 1.0 (refs. 1 and 2, respectively) is presented in figures 10 and 11. For wings having taper ratios of 0.6 and 1.0 the agreement between the calculated and the experimental flutter speeds is shown (fig. 10) to be closer than for the present taper-ratio-0.2 plan form. At supersonic Mach numbers the experimental flutter speeds for all the wings become increasingly greater than the calculated flutter speeds as the Mach number is increased. However, the increase of flutter-speed ratio with Mach number at low supersonic Mach numbers is much more gradual for the wings of higher taper ratio than for the taper-ratio-0.2 wing.

A comparison of the results on the basis of the nondimensional parameter $\dfrac{V_e}{b_s \omega_\alpha \sqrt{\mu_e}}$ (fig. 11) indicates that at subsonic Mach numbers the values change much less when the taper ratio is changed from 1.0 to 0.6 than when the taper ratio is changed from 0.6 to 0.2. At low

supersonic Mach numbers the values of the parameter are about equal for all three wings. However, at the higher supersonic Mach numbers the data again indicate a small effect of taper ratio between taper ratios of 1.0 and 0.6 and a large effect between 0.6 and 0.2. (The nondimensional parameter used in fig. 11 differs slightly from that used in fig. 5 and table II in that fig. 11 employs μ_e for the mass ratio whereas fig. 5 employs $\bar{\mu}_e$. The two expressions for the mass ratio are defined in the list of symbols.)

The fact that the values of $\dfrac{V_e}{b_s \omega_\alpha \sqrt{\mu_e}}$ are lower (fig. 11) for the taper-ratio-0.2 plan form than for the wings of higher taper ratio does not necessarily indicate that the taper-ratio-0.2 plan form is more susceptible to flutter than the other wings. The reason for this is that in the design of an aircraft certain aerodynamic and structural requirements must be satisfied for all plan forms being considered and thus the denominator of the nondimensional parameter is not known until suitable design analyses have been made. The significant result shown by the data in figure 11, and also in figure 10, is that the flutter characteristics of a $45°$, aspect-ratio-4 plan form change appreciably more between taper ratios of 0.6 and 0.2 than between 0.6 and 1.0.

CONCLUSIONS

The results of an investigation of the transonic flutter character-istics of an aspect-ratio-4, $45°$ sweptback plan form having a taper ratio of 0.2, and thickness ratios of 0.03 and 0.04 indicate the following conclusions:

1. A rapid increase in a flutter parameter $\dfrac{V_e}{b_s \omega_\alpha \sqrt{\bar{\mu}_e}}$ and the ratio of flutter frequency to first torsion frequency occurred as the Mach number was increased between $M = 1.05$ and $M = 1.1$ and suggested a rather marked change in the flutter mode.

2. Calculated flutter speeds based on incompressible aerodynamic coefficients were higher than experimental values by about 20 percent or more throughout the subsonic Mach number range of the investigation (from Mach numbers of about 0.65 to 1.0). Calculated flutter frequencies were about 7 percent too high at Mach number 0.65 and about 20 percent too high at Mach number 0.9.

3. The differences in overall stiffness level between the 3- and 4-percent-thick models resulted in considerably reduced values of dynamic pressure required for flutter for the 3-percent-thick models in comparison

with the 4-percent-thick models. The correlation of the data on the basis of $\dfrac{V_e}{b_s \omega_\alpha \sqrt{\bar{\mu}_e}}$ suggested that there were no significant independent effects of thickness ratio on the flutter characteristics of the plan form investigated for the values of thickness ratio employed.

4. A comparison of the results of the present wing with other plan forms which differed only in taper ratio indicated that the flutter characteristics of a 45° sweptback, aspect-ratio-4 plan form change appreciably more between taper ratios of 0.6 and 0.2 than between 0.6 and 1.0.

Langley Research Center,
    National Aeronautics and Space Administration,
        Langley Field, Va. August 13, 1959.

<div align="center">REFERENCES</div>

1. Unangst, John R., and Jones, George W., Jr.: Some Effects of Sweep and Aspect Ratio on the Transonic Flutter Characteristics of a Series of Thin Cantilever Wings Having a Taper Ratio of 0.6. NACA RM L55I13a, 1956.

2. Ruhlin, Charles L.: Experimental Transonic Flutter Characteristics of an Untapered, 45° Sweptback, Aspect-Ratio-4 Wing. NACA RM L55L22, 1956.

3. Lamb, J. J., Boswell, Isabelle, and Axilrod, B. M.: Tensile and Compressive Properties of Laminated Plastics at High and Low Temperatures. NACA TN 1550, 1948.

4. Barmby, J. G., Cunningham, H. J., and Garrick, I. E.: Study of Effects of Sweep on the Flutter of Cantilever Wings. NACA Rep. 1014, 1951. (Supersedes NACA TN 2121.)

5. Houbolt, John C., and Anderson, Roger A.: Calculation of Uncoupled Modes and Frequencies in Bending or Torsion of Nonuniform Beams. NACA TN 1522, 1948.

6. Bisplinghoff, Raymond L., Ashley, Holt, and Halfman, Robert L.: Aeroelasticity. Addison-Wesley Pub. Co., Inc. (Cambridge, Mass.), c.1955.

TABLE I.- PHYSICAL PROPERTIES OF MODELS

(a) Models with thickness ratio of 0.03

NACA streamwise section	65A003
A	4
Λ, deg	45
λ	0.2
λ_p	0.242
Span, ft	1.142
A_p	1.83
l, ft	0.630
b_r, ft	0.1725
b_s, ft	0.1979
g_h	0.014

Model 4A - right panel $\bar{m} = 0.0017$ slug

η	a	x_α	r_α^2	m, slugs/ft	$\dfrac{b}{b_r}$
0.05	-0.305	0.203	0.337	0.00706	0.9621
.15	-.268	.166	.311	.00617	.8864
.25	-.231	.128	.284	.00529	.8106
.35	-.192	.088	.258	.00442	.7349
.45	-.149	.046	.232	.00359	.6591
.55	-.102	-.002	.205	.00281	.5834
.65	-.045	-.058	.179	.00211	.5076
.75	.035	-.138	.152	.00153	.4319
.85	.140	-.244	.123	.00110	.3561
.95	.333	-.449	.234	.00078	.2804

Item	Model 1A		Model 2A		Model 3A		Model 4A
	Left	Right	Left	Right	Left	Right	Right
$f_{h,1}$	87.5	88	90	79	89.5	88	96
$f_{h,2}$	285	288	279	239	279	272	313
$f_{h,3}$	660	667	665	570	650	730	698
f_t	530	518	532	516	530	515	547
f_α	494.7	483	496	481.5	494.5	480.5	510
$\omega_{h,1}/\omega_\alpha$	0.177	0.182	0.181	0.164	0.181	0.183	0.188
$\omega_{h,2}/\omega_\alpha$	0.576	0.596	0.562	0.496	0.565	0.566	0.614
$\omega_{h,3}/\omega_\alpha$	1.335	1.381	1.340	1.183	1.315	1.519	1.369

TABLE I.- PHYSICAL PROPERTIES OF MODELS - Concluded

(b) Models with thickness ratio of 0.04

NACA streamwise section	65A004
A	4
Λ, deg	45
λ	0.2
λ_p	0.242
Span, ft	1.142
A_p	1.83
l, ft	0.630
b_r, ft	0.1725
b_s, ft	0.1979
g_h	0.028

Model 1 - left panel $\bar{m}$ = 0.0021 slug

η	a	x_α	r_α^2	m, slugs/ft	$\dfrac{b}{b_r}$
0.05	-0.190	0.036	0.202	0.00948	0.9621
.15	-.166	.020	.206	.00805	.8864
.25	-.144	.006	.210	.00669	.8106
.35	-.122	-.008	.214	.00544	.7349
.45	-.100	-.022	.218	.00433	.6591
.55	-.076	-.038	.224	.00337	.5834
.65	-.048	-.058	.241	.00255	.5076
.75	-.010	-.090	.273	.00188	.4319
.85	.040	-.132	.328	.00136	.3561
.95	.112	-.196	.312	.00097	.2804

Item	Model 1		Model 2	
	Left	Right	Left	Right
$f_{h,1}$	107.5	108	109.5	116
$f_{h,2}$	340	343	345	338
$f_{h,3}$	789	800	790	792
f_t	670	671	690	718
f_α	660	661	680	707
$\omega_{h,1}/\omega_{\alpha,1}$	0.1628	0.1634	0.1609	0.1640
$\omega_{h,2}/\omega_{\alpha,1}$	0.5148	0.5186	0.5070	0.4785
$\omega_{h,3}/\omega_{\alpha,1}$	1.195	1.210	1.162	1.120

TABLE II.- COMPILATION OF ANALYTICAL AND TEST RESULTS

(a) Models with thickness ratio of 0.03

Model	Run	Point	Wing-panel behavior[1] Left	Right	M_e	$\frac{V_e}{V_R}$	ρ_e, slugs/cu ft	μ_e	f_α, cps	f_e, cps	$\frac{f_e}{f_\alpha}$	$\frac{\omega_e}{\omega_R}$	V_e, ft/sec	$\frac{V_e}{b_s\omega_\alpha\sqrt{\mu_e}}$	q_e, lb/sq in.	k_T
1A	1	1	F_1	F_1	0.720	0.798	0.0021	41.79	488.8	215	0.440	0.905	787.0	0.2221	4.58	0.4187
	2	1	F_1	F_1	.740	.809	.0020	43.88	488.8	210	.430	.893	810.5	.2236	4.58	.3971
		2	E_1	E_1	1.072	1.080	.0018	48.75	488.8	240	.492	1.047	1,115.2	.2917	7.57	.3306
		3	D_2	D_2	1.329	1.531	.0034	25.81	488.8	---	-----	-----	1,287.3	.4624	19.86	------
		4	F_2	F_2	1.331	1.587	.0038	23.09	488.8	478	.978	1.755	1,284.1	.4879	21.60	.5706
	3	1	F_1	F_1	.639	.808	.0030	29.25	488.8	24:	.493	.932	708.9	.2392	5.23	.5211
	4	1	E_1	E_1	1.054	1.160	.0024	36.56	488.8	25(	.512	1.021	1,096.8	.3311	9.85	.3494
		2	F_2	F_2	1.388	1.599	.0035	25.07	488.8	469	.960	1.751	1,331.5	.4853	21.40	.5399
	5	1	F_1	F_1	.714	.812	.0022	39.89	488.8	216	.442	.900	790.2	.2283	4.68	.4190
		2	E_1	E_1	1.071	1.166	.0022	39.89	488.8	250	.511	1.042	1,134.5	.3277	9.96	.3378
		3	D_2	D_2	1.369	1.546	.0031	28.31	488.8	---	-----	-----	1,340.5	.4598	19.55	------
		4	F_2	F_2	1.388	1.585	.0033	26.59	488.8	464	.949	1.758	1,345.7	.4762	21.06	.5285
	6	1	F_1	F_1	.714	.809	.0022	39.89	488.8	218	.446	.908	787.0	.2274	4.68	.4246
		2	E_1	E_1	1.063	1.106	.0020	43.88	488.8	234	.479	.995	1,107.6	.3052	8.71	.3238
		3	D_2	D_2	1.294	1.494	.0032	27.42	488.8	---	-----	-----	1,282.4	.4469	18.13	------
		4	F_2	F_2	1.300	1.533	.0035	25.07	488.8	46?	.945	1.724	1,276.9	.4654	19.71	.5546
	7	1	F_1	F_1	.678	.778	.0022	39.89	488.8	21?	.446	.908	757.4	.2188	4.46	.4412
		2	E_1	E_1	1.071	1.174	.0023	38.15	488.8	23?	.489	.986	1,126.0	.3327	9.96	.3253
		3	D_2	D_2	1.211	1.434	.0032	27.42	488.8	---	-----	-----	1,231.1	.4290	17.11	------
		4	F_2	F_2	1.214	1.473	.0035	25.07	488.8	46?	.960	1.751	1,226.6	.4471	18.36	.5861
	8	1	F_1	F_1	.711	.819	.0022	39.89	488.8	21?	.446	.906	797.4	.2304	4.99	.4190
		2	E_1	E_1	1.073	1.200	.0025	35.10	488.8	28?	.583	1.152	1,118.5	.3446	10.93	.3906
		3	D_2	D_2	1.140	1.305	.0028	31.34	488.8	---	-----	-----	1,171.7	.3817	13.56	------
		4	F_2	F_2	1.163	1.368	.0031	28.31	488.8	43?	.890	1.670	1,186.4	.4067	15.24	.5620
2A	9	1	F_1	F_1	.674	.788	.0023	38.15	489.1	22?	.454	.915	756.9	.2234	4.56	.4496
		2	F_2	F_2	1.093	1.271	.0028	31.34	489.1	40?	.828	1.593	1,141.7	.3718	12.70	.5437
3A	10	1	F_1	F_1	.674	.796	.0023	38.15	487.3	22?	.462	.931	761.0	.2254	4.56	.4532
		2a	E_1	E_1	1.062	1.227	.0028	31.34	487.3	25?	.513	.986	1,098.4	.3590	11.64	.3489
		2b	F_2	F_2	1.062	1.227	.0028	31.34	487.3	40?	.831	1.598	1,098.4	.3590	11.64	.5652
		3			1.096	1.290	.0030	29.25	487.3	42?	.867	1.642	1,128.3	.3818	13.31	.5740
		4			1.102	1.305	.0031	28.31	487.3	43?	.888	1.667	1,128.7	.3883	13.94	.5880
		5a	E_2	E_2	1.055	1.289	.0034	25.81	487.3	41?	.858	1.577	1,080.2	.3892	13.63	.5931
		5b	F_3	F_3	1.055	1.289	.0034	25.81	487.3	26?	.542	.996	1,080.2	.3892	13.63	.3746

[1]Wing-panel behavior code:
  F - flutter
  E - end of flutter (dynamic pressure increasing)
  D - low damping

Subscripts:
  1 - associated with first occurrence of flutter
  2 - associated with second occurrence of flutter
  3 - associated with third occurrence of flutter

TABLE II.- COMPILATION OF ANALYTICAL AND TEST RESULTS - Concluded

(b) Models with thickness ratio of 0.04

Model	Run	Point	Wing-panel behavior[1] Left	Right	M_e	$\frac{V_e}{V_R}$	ρ_e, slugs/cu ft	μ_e	f_α, cps	f_e, cps	$\frac{f_e}{f_\alpha}$	$\frac{\omega_e}{\omega_R}$	V_e, ft/sec	$\frac{V_e}{b_s\omega_\alpha\sqrt{\mu_e}}$	q_e, lb/sq in.	k_r
1	11	1	F_1	F_1	0.937	0.747	0.0025	43.13	660	247	0.374	0.822	967.8	0.1986	8.28	0.3920
		2	E_1		.989	.788	.0026	41.47	660	245	.371	.805	1,010.5	.2116	9.22	.3715
		3		E_1	.997	.792	.0026	41.47	661	250	.378	.821	1,017.2	.2126	9.38	.3768
		4	M'	M'	1.181	1.203	.0072	14.98	660	---	-----	-----	1,096.9	.3819	30.03	------
	12	1	F_1	F_1	.913	.742	.0026	41.47	660	256	.388	.840	952.2	.1992	8.32	.4120
		2	E_1	E_1	.986	.802	.0028	38.51	660	262	.397	.844	1,010.4	.2194	10.02	.3974
		3	M'	M'	1.103	1.165	.0080	13.48	660	---	-----	-----	1,021.7	.3748	29.04	------
	13	1	E_1	E_1	1.026	.832	.0031	34.78	660	272	.412	.854	1,016.4	.2321	11.11	.4102
		2	F_2		1.075	.887	.0034	31.71	660	300	.454	.920	1,053.4	.2521	13.23	.4365
		3		F_2	1.090	.984	.0046	23.44	661	343	.519	.981	1,058.3	.2942	17.74	.4968
	14	1	F_1	F_1	.898	.735	.0029	37.18	660	248	.376	.794	916.6	.2024	8.50	.4154
		2		E_1	.987	.807	.0031	34.78	661	269	.407	.844	988.1	.2255	10.58	.4169
		3	E_1		1.001	.819	.0031	34.78	660	276	.418	.868	999.8	.2286	10.89	.4231
		4	F_2		1.068	.885	.0034	31.71	660	296	.448	.908	1,050.6	.2515	13.08	.4319
	15	1	F_1	F_1	.819	.753	.0041	26.30	660	289	.438	.848	841.6	.2211	10.01	.5264
	16	1	F_1	F_1	.826	.780	.0046	23.44	660	300	.454	.859	837.8	.2331	11.16	.5489
	17	1	F_1	F_1	.759	.760	.0054	19.97	660	305	.462	.846	771.2	.2325	11.07	.6061
	18	1	F_1	F_1	.822	.745	.0038	28.37	660	285	.432	.851	853.0	.2158	9.56	.5122
	19	1	F_1	F_1	.785	.770	.0048	22.46	660	304	.461	.862	814.8	.2316	11.17	.5718
	20	1	F_1	F_1	.888	.728	.0027	39.93	660	247	.374	.804	925.3	.1972	8.12	.4100
		2	E_1	E_1	.970	.790	.0028	38.51	660	268	.406	.864	995.1	.2159	9.69	.4121
		3	M'	M'	1.096	1.159	.0071	15.19	660	---	-----	-----	1,063.0	.3680	28.03	------
2	21	1	F_1	F_1	.897	.701	.0027	39.93	693	259	.374	.801	935.6	.1899	8.25	.4242
		2	E_1	E_1	.960	.755	.0029	37.18	693	---	-----	-----	989.1	.2081	9.74	------
		3		F_2	1.075	1.001	.0056	19.25	707	525	.742	1.350	1,072.8	.3076	22.21	.7502
	22	1	F_1	F_1	.871	.681	.0026	41.47	693	248	.358	.776	917.8	.1830	7.60	.4141
		2		E_1	.973	.734	.0026	41.47	707	248	.351	.761	1,009.0	.1971	9.17	.3767
		3	E_1		.981	.768	.0026	41.47	679	248	.365	.792	1,014.7	.2063	9.33	.3746
		4	M'	M'	1.128	1.120	.0068	15.86	693	---	-----	-----	1,095.1	.3529	28.50	------
	23	1	F_1	F_1	.948	.735	.0026	41.47	693	255	.368	.798	990.8	.1974	8.71	.3944
		2	E_1	E_1	.985	.767	.0027	39.93	693	255	.368	.790	1,024.4	.2082	9.71	.3815
		3		F_2	1.079	1.027	.0062	17.39	707	558	.789	1.409	1,060.5	.3201	24.42	.8065
	24	1	F_1	F_1	.906	.710	.0026	41.47	693	253	.365	.792	956.6	.1906	8.42	.4055
		2	E_1	E_1	.993	.773	.0027	39.93	693	253	.365	.785	1,032.3	.2096	9.87	.3757
		3		F_2	1.071	.986	.0053	20.34	707	520	.736	1.349	1,077.6	.3006	21.39	.7396
		4	F_2		1.060	1.048	.0058	18.59	679	394	.580	1.047	1,064.6	.3234	22.88	.5674
		5	E_2		1.066	1.062	.0060	17.97	679	400	.589	1.057	1,065.5	.3290	23.83	.3295
		6	F_3		1.066	1.099	.0067	16.09	679	512	.754	1.326	1,058.3	.3455	26.13	.7416

[1]Wing-panel behavior code:
F - flutter
E - end of flutter (dynamic pressure increasing)
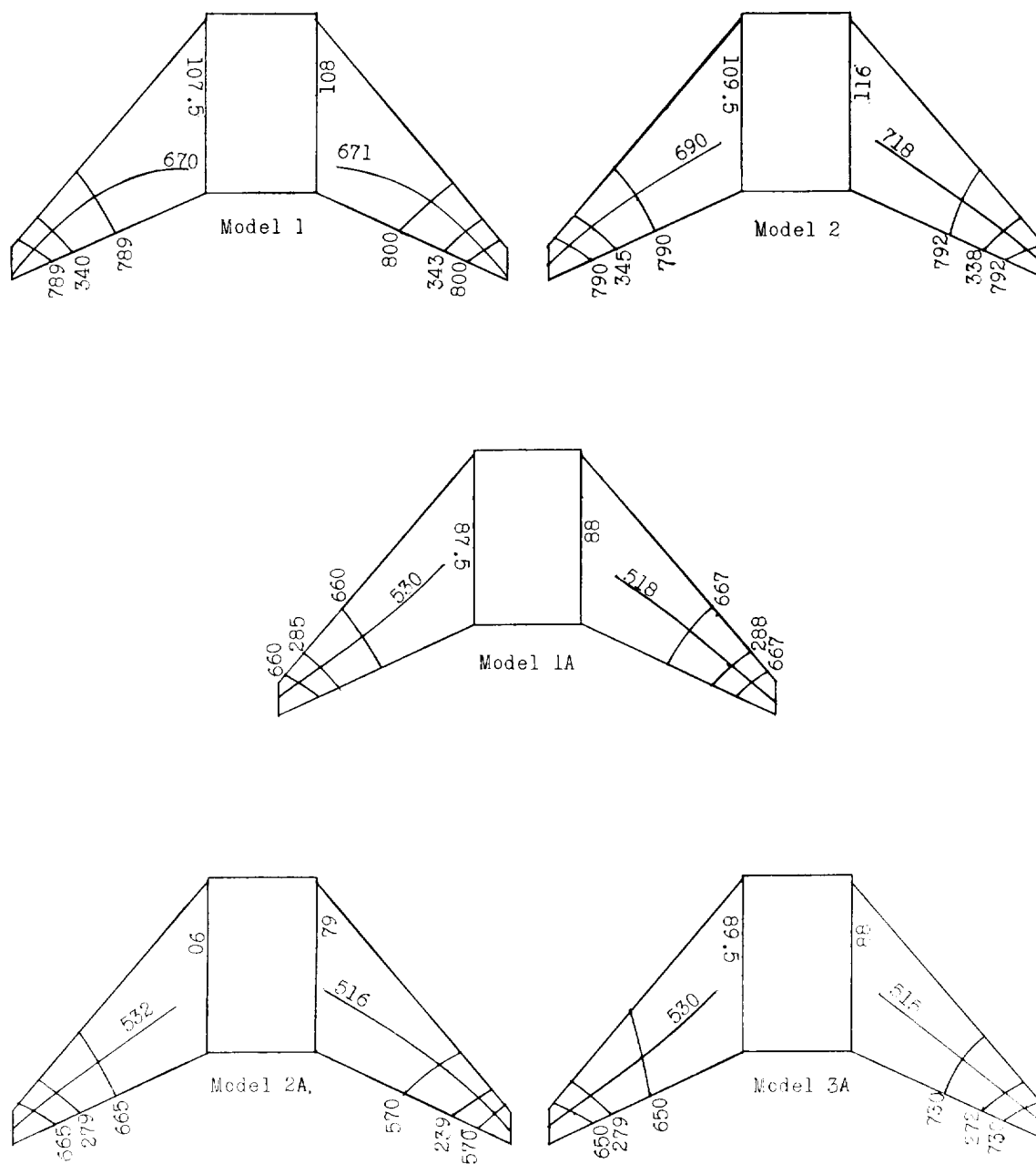M' - maximum dynamic pressure, no flutter

Subscripts:
1 - associated with first occurrence of flutter
2 - associated with second occurrence of flutter
3 - associated with third occurrence of flutter

18
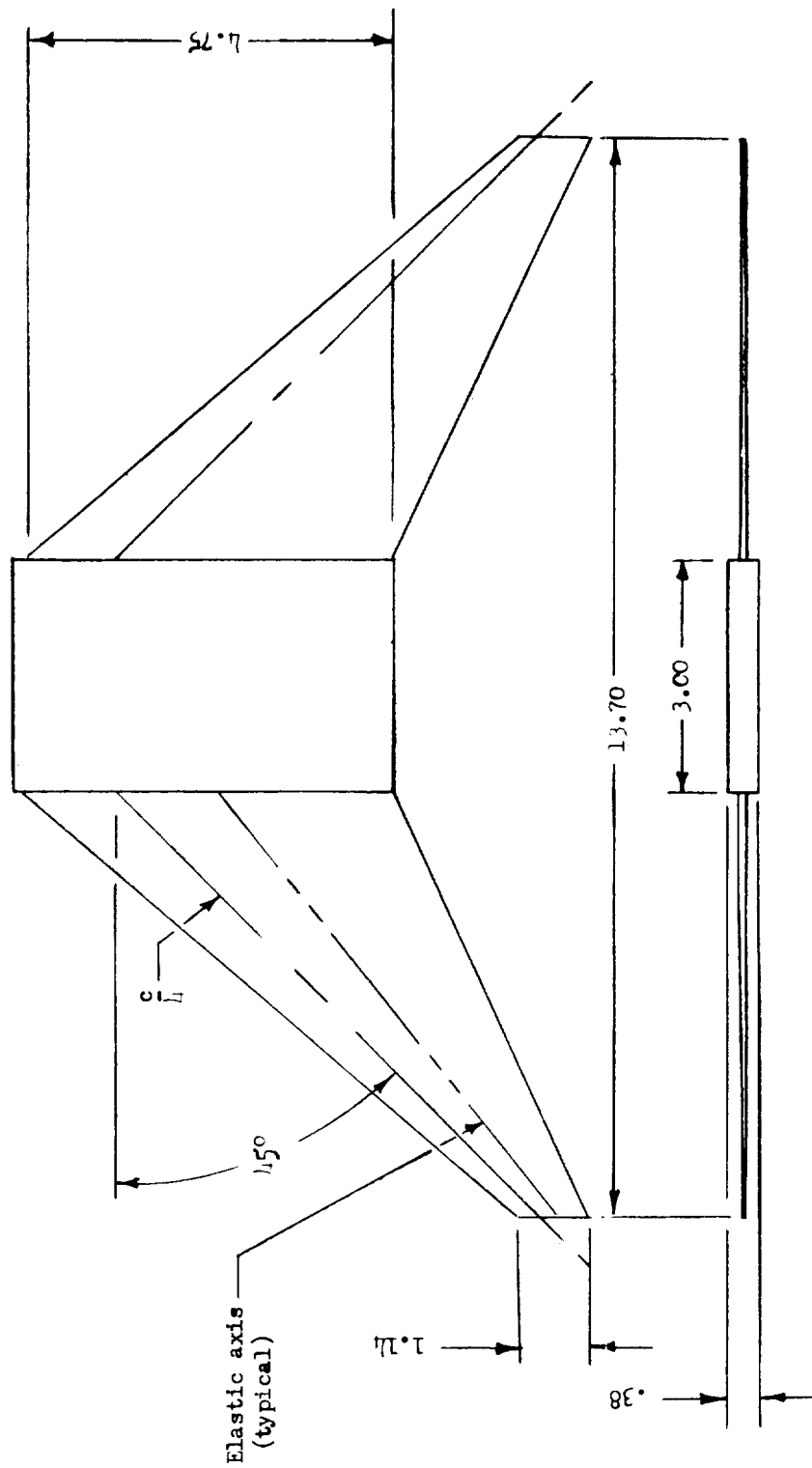
(a) Dimensions of model in inches.

Figure 1.- Drawings of flutter models showing dimensions, node lines, and associated natural-vibration frequencies.

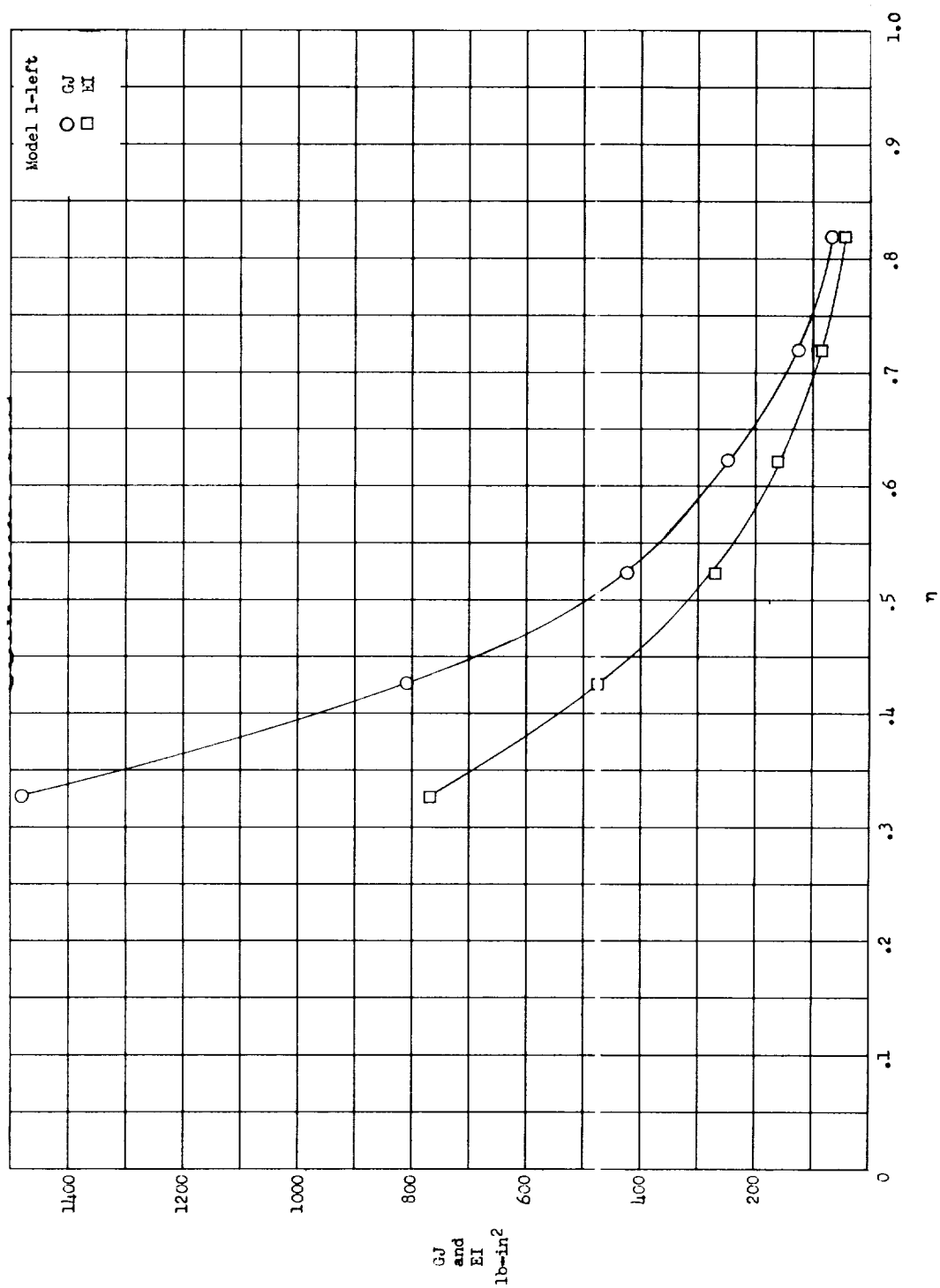(b) Node lines and associated natural frequencies.

Figure 1.- Concluded.

Figure 2.- Measured spanwise variation of bending and torsional stiffnesses for model 1, left wing panel.
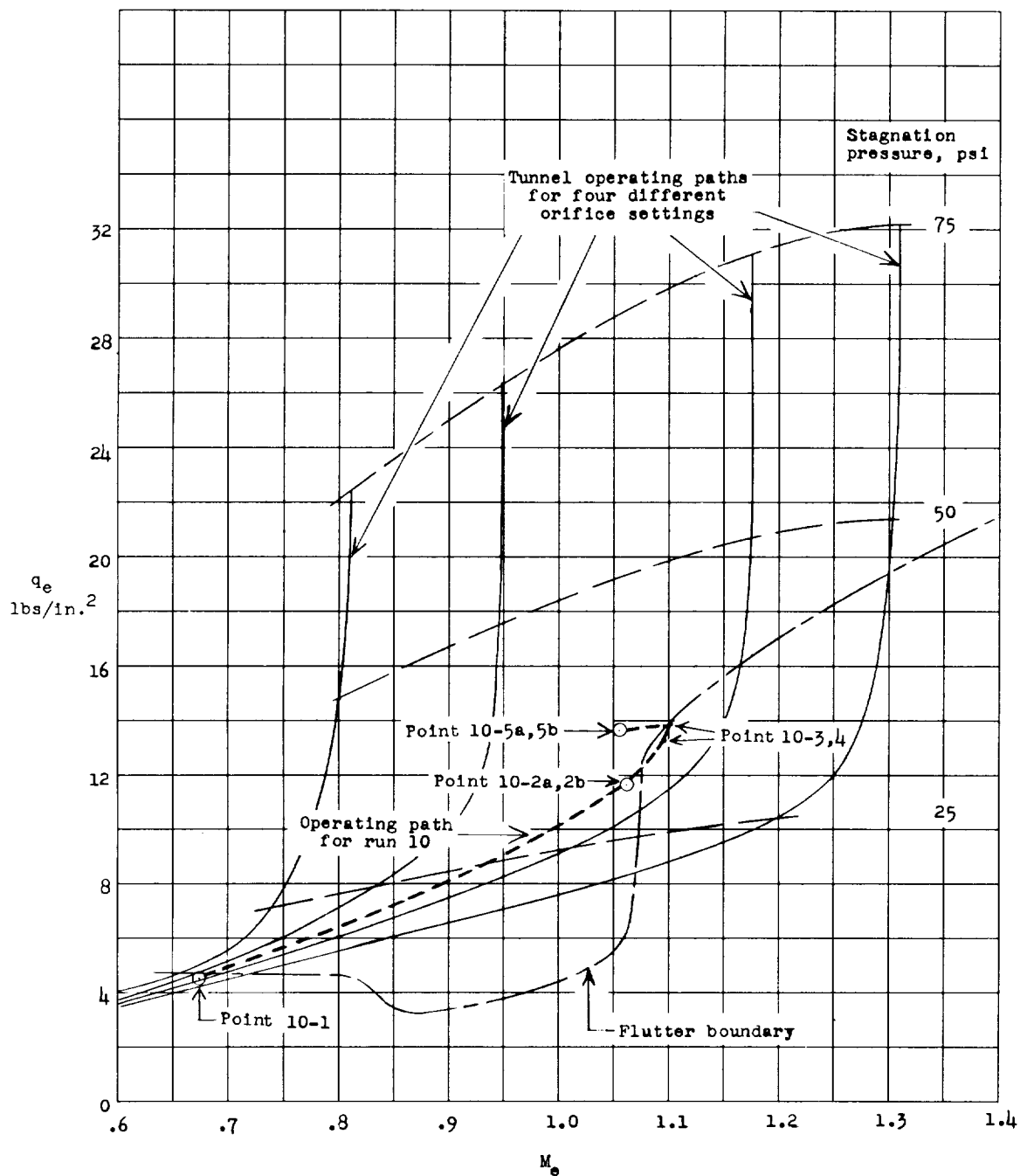
Figure 3.- Operating characteristics of the 26-inch Langley transonic blowdown tunnel. Also shown is a hypothetical flutter boundary and a test run. Identification of points are shown in columns 2 and 3 of table II.
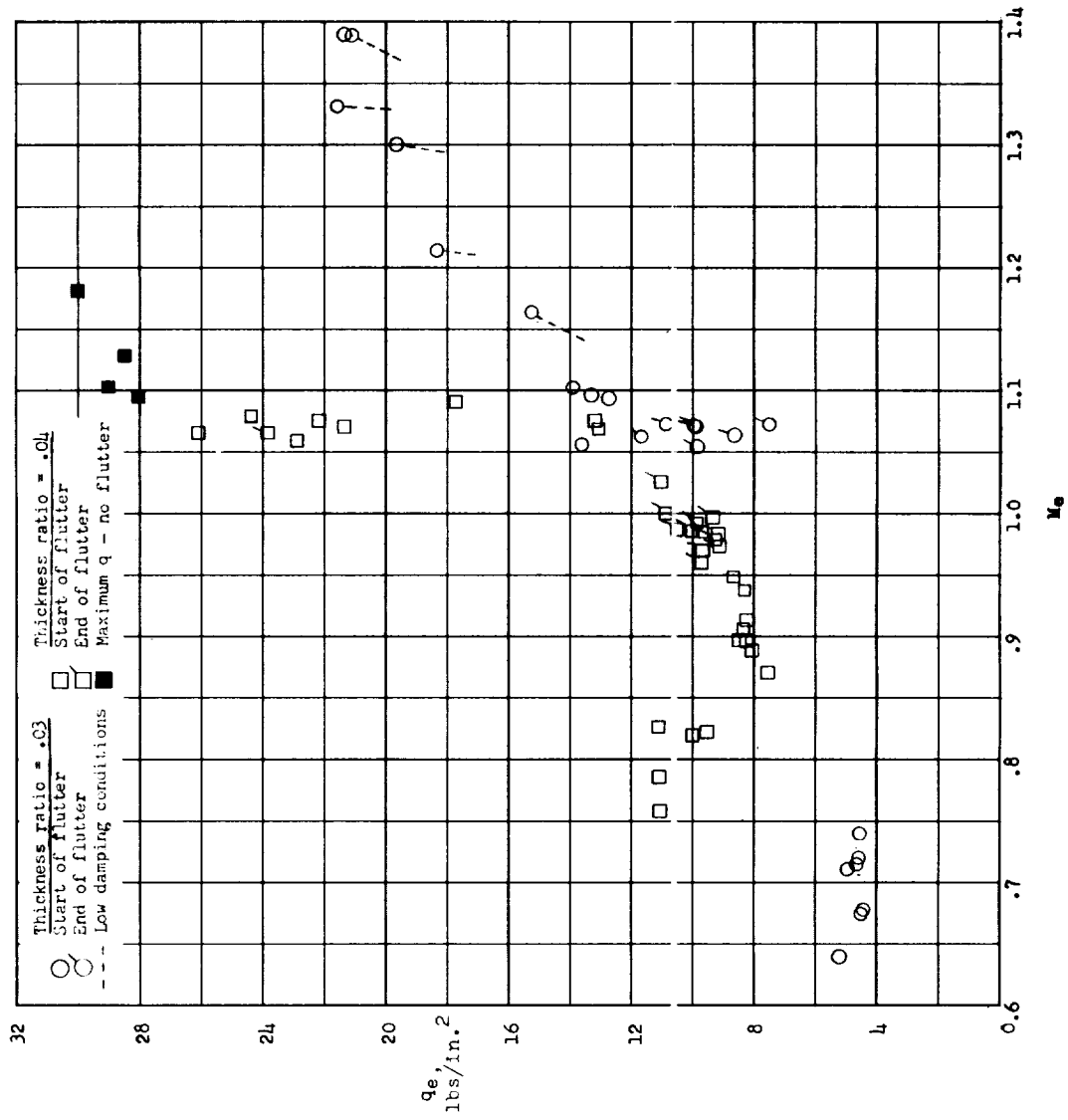
Figure 4.- Variation with Mach number of the dynamic pressure required for flutter.
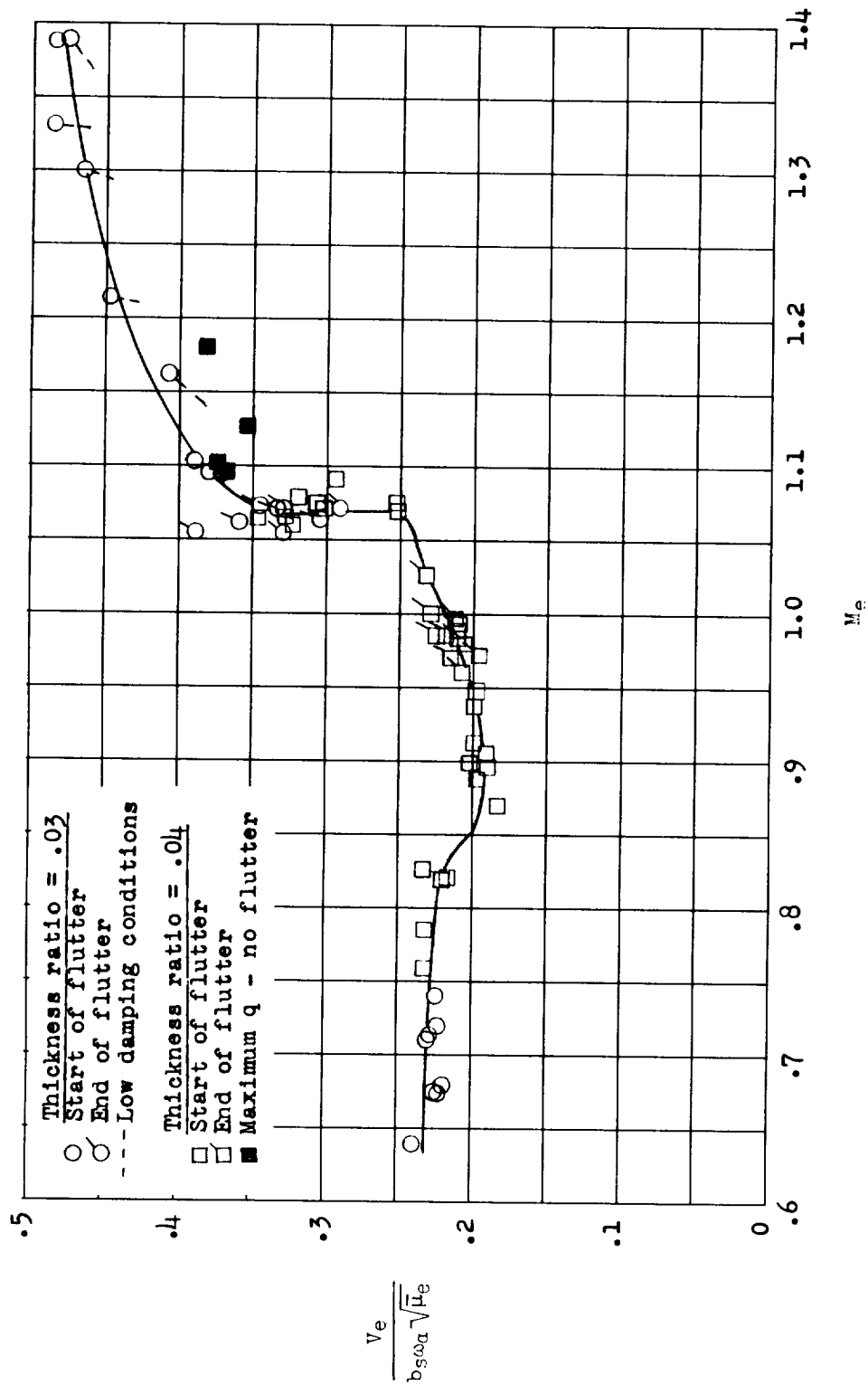
Figure 5.- Variation of the experimental coefficient $\dfrac{V_e}{b_s \omega_\alpha \sqrt{\mu_e}}$ with Mach number.
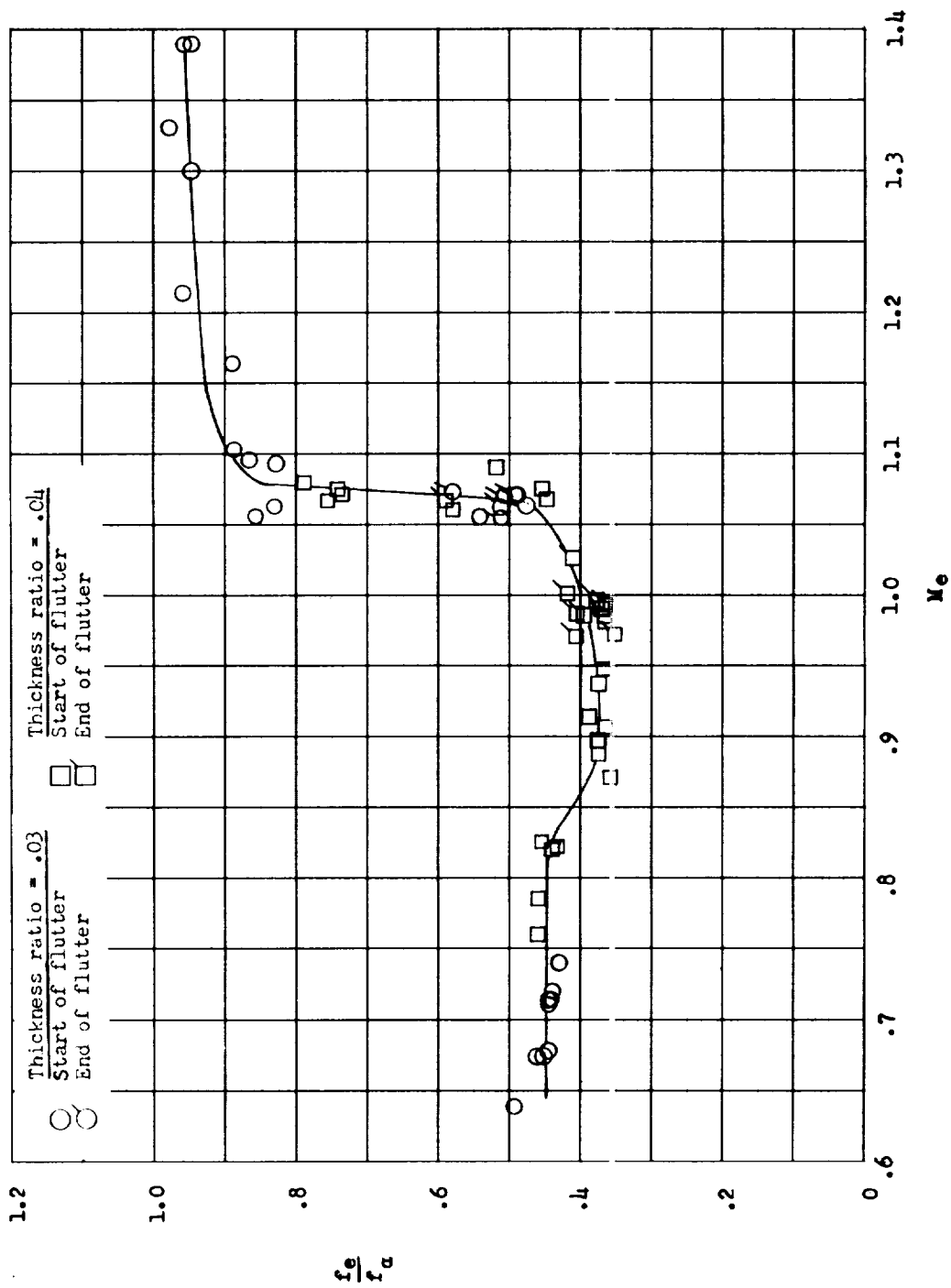
Figure 6.- Variation with Mach number of the ratio of the experimental flutter frequencies to the uncoupled torsion frequencies.
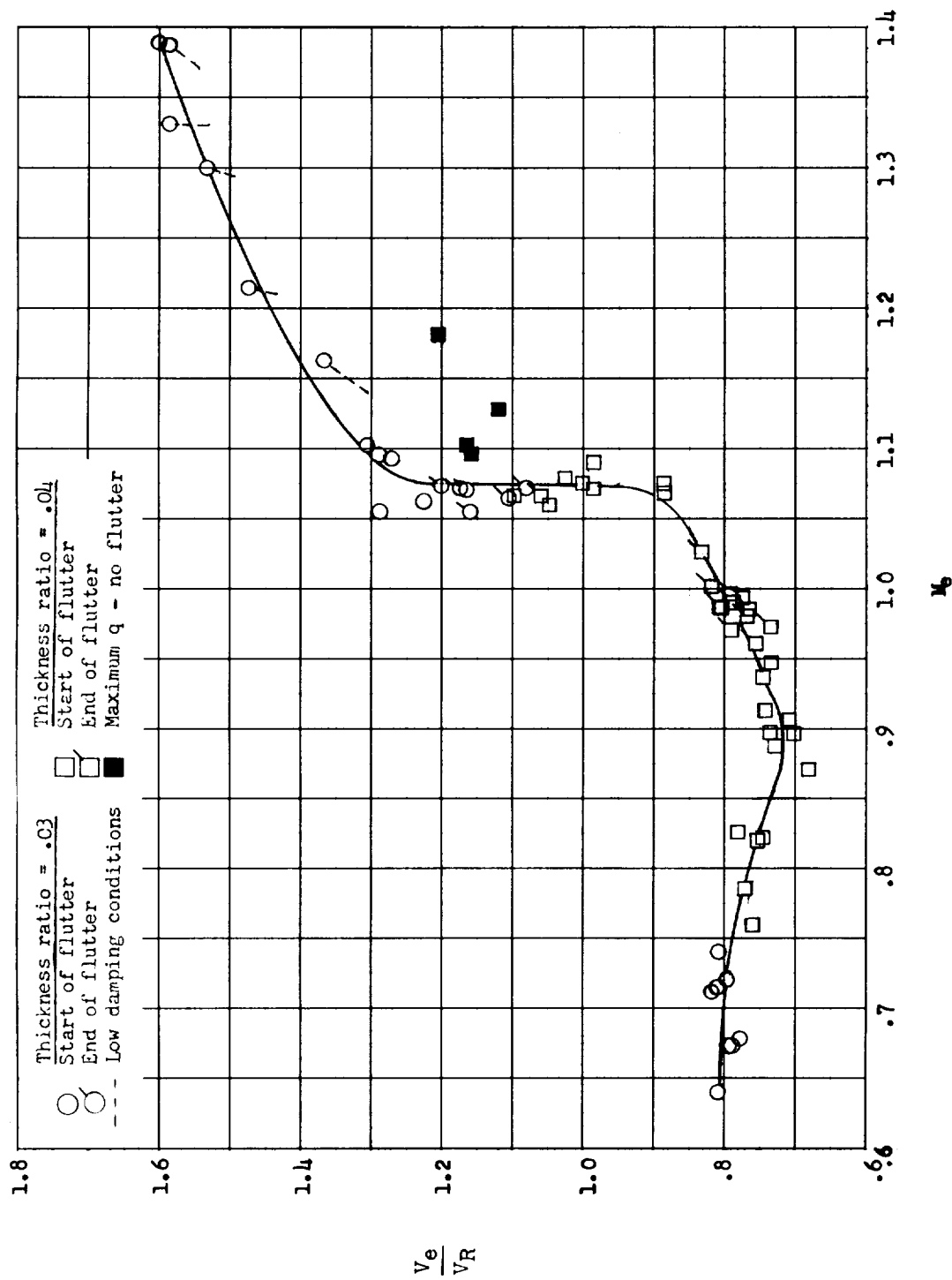
Figure 7.- Variation of the flutter-speed ratio with Mach number for the taper-ratio-0.2 wings.
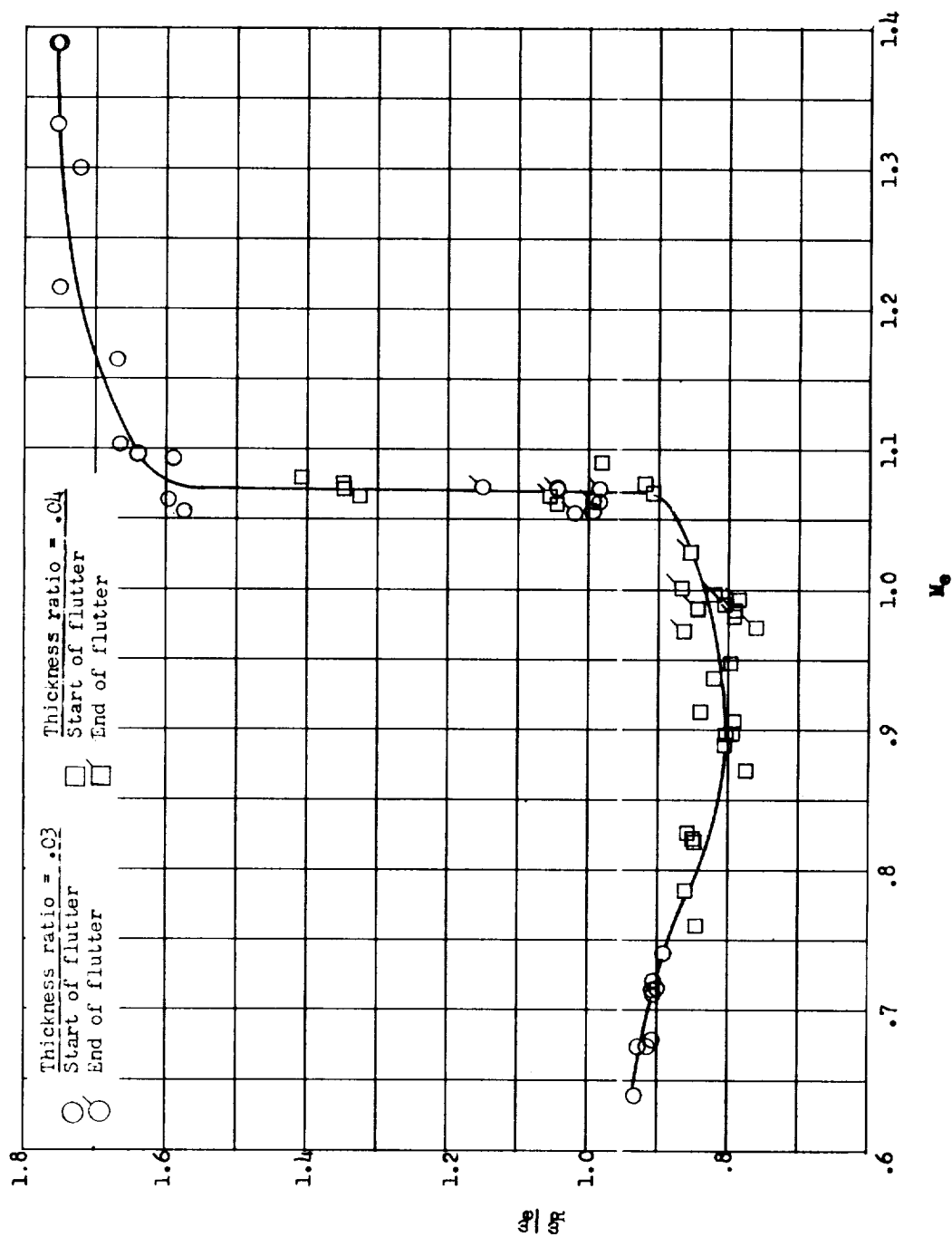
Figure 8.- Variation of the ratio of experimental to calculated flutter frequencies with Mach number for the taper-ratio-0.2 wings.
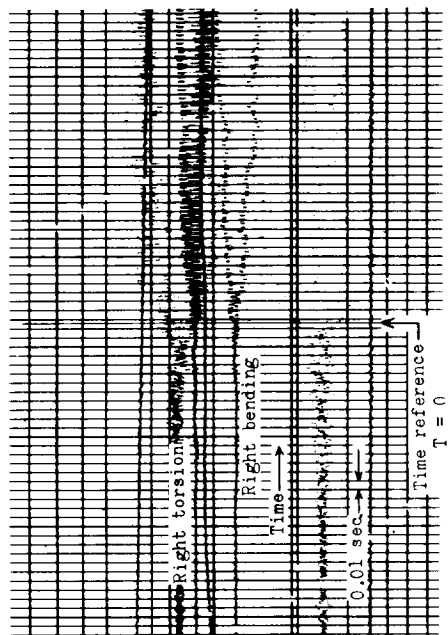
(a) Point 10-1. M_e = 0.674;
f_e = 225 cps.
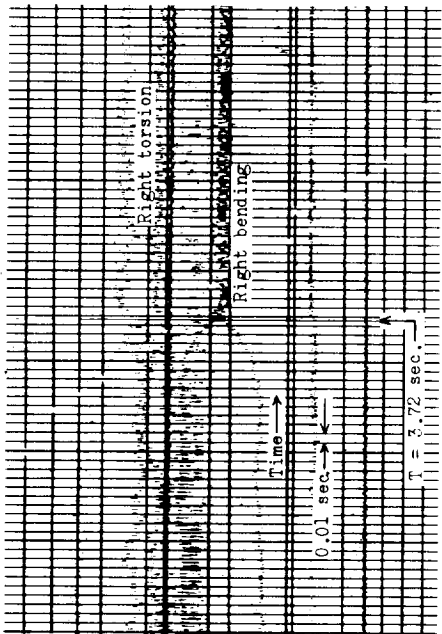
(b) Point 10-2a, 2b. M_e = 1.062;
$f_{e,a}$ = 250 cps; $f_{e,b}$ = 405 cps.
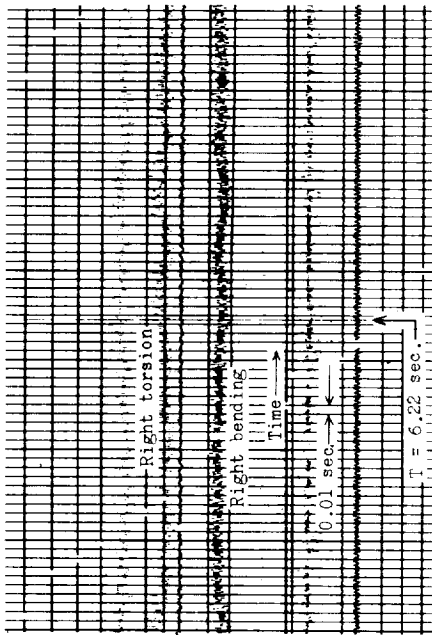
(c) Point 10-4. M_e = 1.102;
f_e = 433 cps.
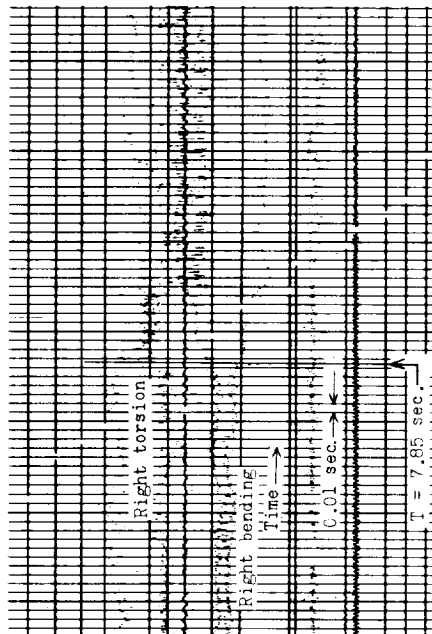
(d) Point 10-5a, 5b. M_e = 1.055;
$f_{e,a}$ = 418 cps; $f_{e,b}$ = 264 cps.

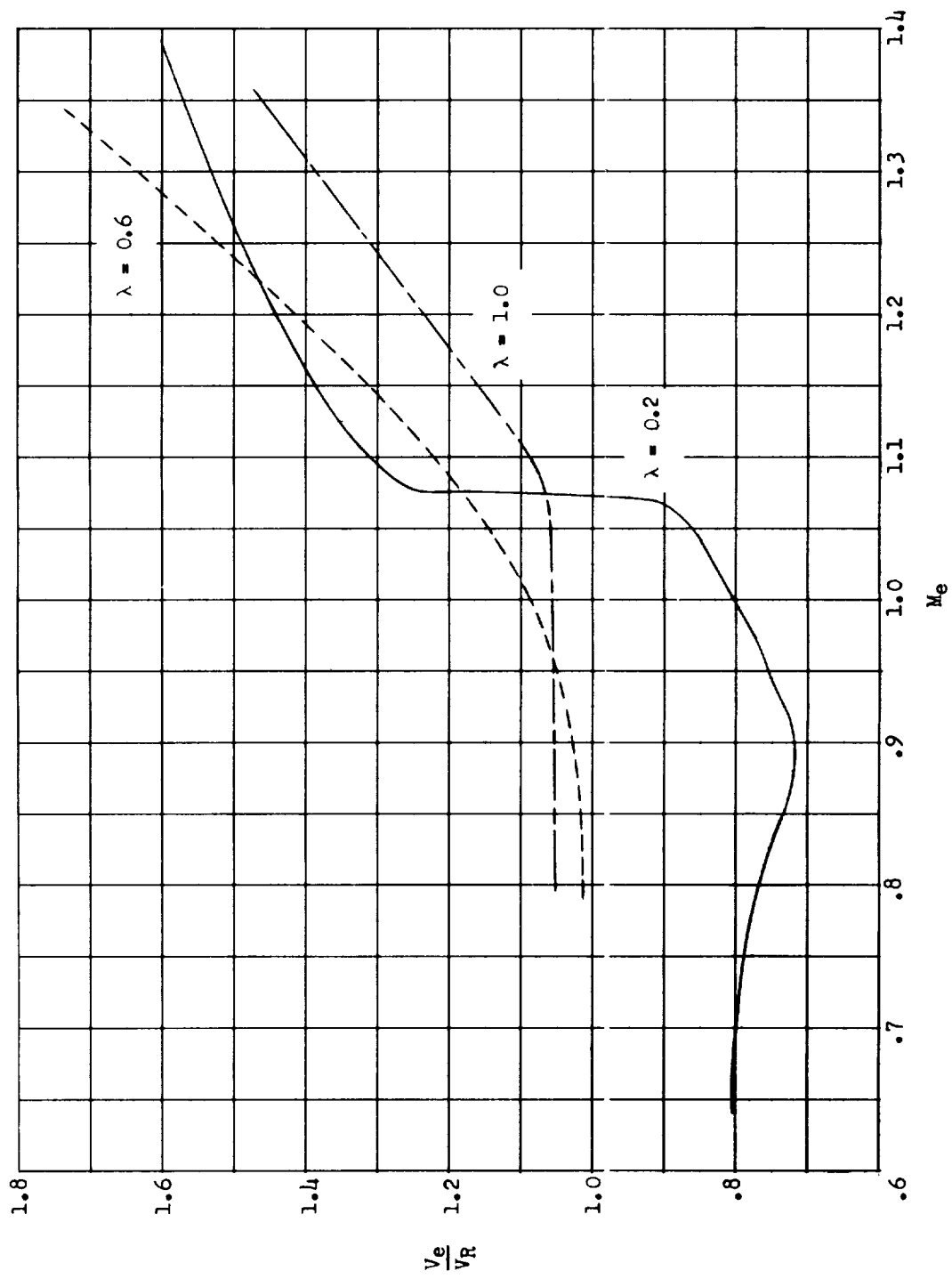Figure 9.- Samples of oscillograph record taken during run 10.

Figure 10.- Comparison of flutter-speed ratios for wings with taper ratios 0.2, 0.6, and 1.0.
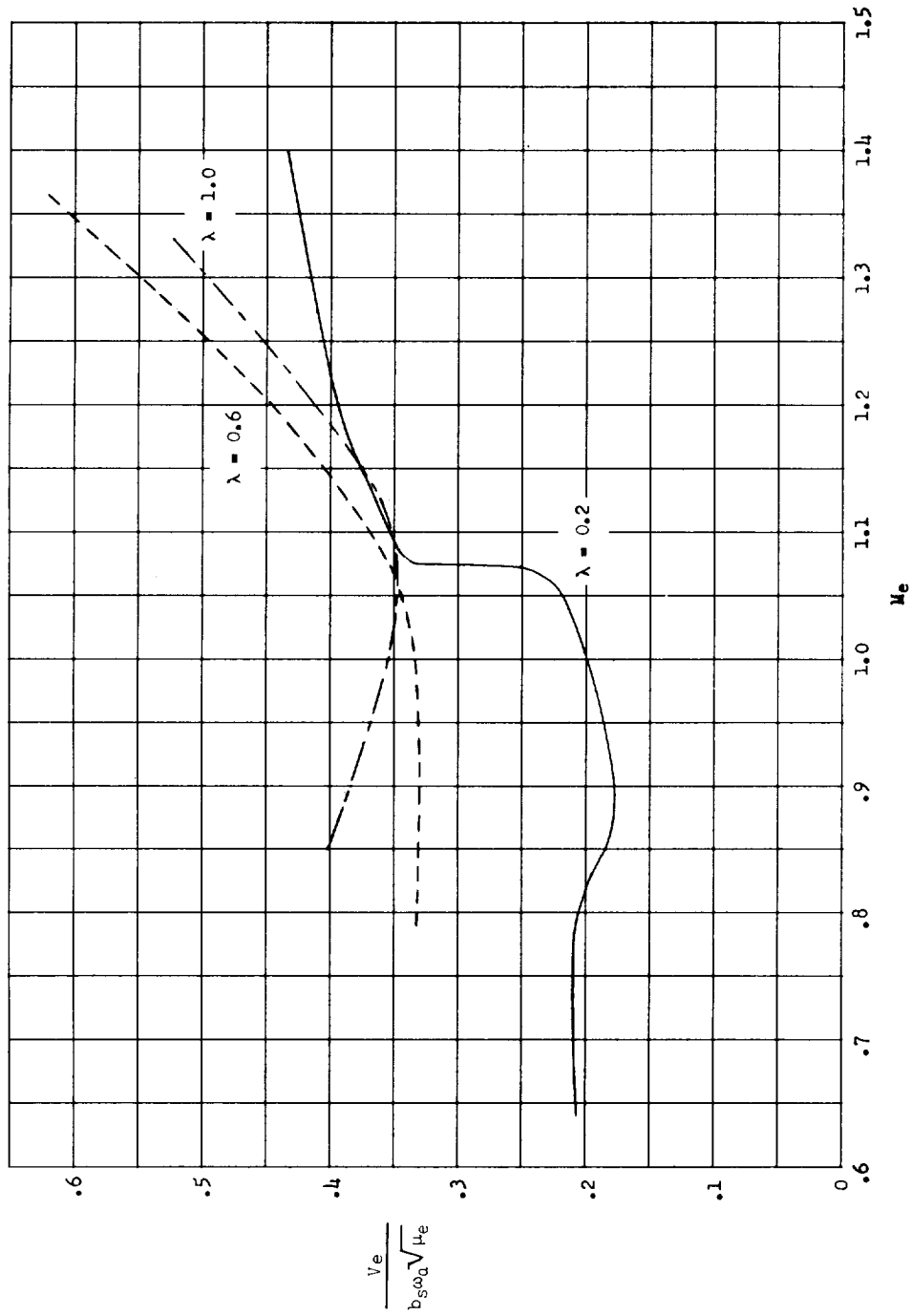
Figure 11.- Comparison of the experimental coefficient $\dfrac{V_e}{b_s \omega_\alpha \sqrt{\mu_e}}$ for wings with taper ratios of 0.2, 0.6, and 1.0.